

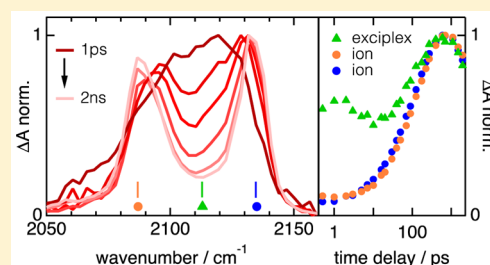
Bimodal Exciplex Formation in Bimolecular Photoinduced Electron Transfer Revealed by Ultrafast Time-Resolved Infrared Absorption

Marius Koch,[†] Giuseppe Licari, and Eric Vauthey*

Department of Physical Chemistry, University of Geneva, 30 Quai Ernest-Ansermet, CH-1211 Geneva 4, Switzerland

S Supporting Information

ABSTRACT: The dynamics of a moderately exergonic photoinduced charge separation has been investigated by ultrafast time-resolved infrared absorption with the dimethylantracene/phthalonitrile donor/acceptor pair in solvents covering a broad range of polarity. A distinct spectral signature of an exciplex could be identified in the $\text{C}\equiv\text{N}$ stretching region. On the basis of quantum chemistry calculations, the 4–5 times larger width of this band compared to those of the ions and of the locally excited donor bands is explained by a dynamic distribution of exciplex geometry with different mutual orientations and distances of the constituents and, thus, with varying charge-transfer character. Although spectrally similar, two types of exciplexes could be distinguished by their dynamics: short-lived, “tight”, exciplexes generated upon static quenching and longer-lived, “loose”, exciplexes formed upon dynamic quenching in parallel with ion pairs. Tight exciplexes were observed in all solvents, except in the least polar diethyl ether where quenching is slower than diffusion. The product distribution of the dynamic quenching depends strongly on the solvent polarity: whereas no significant loose exciplex population could be detected in acetonitrile, both exciplex and ion pair are generated in less polar solvents, with the relative population of exciplex increasing with decreasing solvent polarity. These results are compared with those reported previously with donor/acceptor pairs in different driving force regimes to obtain a comprehensive picture of the role of the exciplexes in bimolecular photoinduced charge separation.



INTRODUCTION

Since their first observation by Leonhardt and Weller in 1963,¹ exciplexes have been found to play a crucial role in many photoinduced charge-transfer processes.^{2–5} They have indeed been invoked in intra-^{6–10} and intermolecular electron transfer in solution,^{11–17} in organic semiconductors for photovoltaics^{18–23} and organic light-emitting diodes,^{24–28} and in biological systems like DNA^{29–32} and photosynthetic reaction centers,³³ sometimes under different names, such as charge-transfer excitons or excited charge-transfer complexes. All these monikers designate a species with an electronic structure between those of the reactants and products. In other words, an exciplex can be viewed as the result of an incomplete photoinduced charge separation (CS). Its formation and nature depends on several key factors such as the CS driving force, $-\Delta G_{\text{CS}}$, the polarity of the environment, and the distance between the electron donor (D) and acceptor (A). Partial charge transfer needs some spatial overlap of molecular orbitals of D and A, and it is thus present only at short distance. However, in liquid solution, bimolecular CS requires first the diffusion of the reactants and, if ΔG_{CS} is significantly negative, CS can take place before D and A have reached a distance and/or a relative orientation with a large orbital overlap, i.e., before a large electronic coupling is achieved.^{34–38} This situation favors full charge separation, i.e., the formation of a radical ion pair rather than an exciplex (assuming that D and A are neutral closed-shell species). Such direct formation of ion pairs mainly takes place in highly polar solvents, where large driving forces

can be easily achieved as a result of the stabilization of the ion pair product by solvation. On the other hand, exciplex formation is favored when ΔG_{CS} is small, because of the nature of D and A and/or the weak polarity of the environment. In these cases, CS is possible only at short distance where both the electronic coupling and the Coulombic interaction are large and compensate for the small solvation energy. In solids, the frequently low polarity of the environment and close distance between the reactants favor the formation of an exciplex, or a charge-transfer exciton. The dissociation of such an exciton into free charge carriers requires the Coulombic attraction to be overcome. This is a crucial step that limits the efficiency of many photovoltaic systems.^{39–42} As a consequence, a deep knowledge of the role of exciplexes in bimolecular photoinduced CS processes in environments of varying polarity is important not only for our basic understanding of electron-transfer processes but also for practical applications.

Exciplexes are spectroscopically elusive species. Their electronic absorption spectra are very similar to those of the ion pairs; thus, the distinction between these two intermediates is problematic.^{5,43–45} In general, exciplexes are detected by their emission. However, because of their substantial charge-transfer character, the radiative rate constant is much smaller than that

Received: August 7, 2015

Revised: August 11, 2015

Published: August 12, 2015

of the local fluorescence of the excited reactant. Consequently, measuring the ultrafast exciplex dynamics by gating techniques is generally not feasible. Insight into the nature of the primary quenching product, i.e., exciplex or ion pair, can be obtained by studying the effect of an external magnetic field on the nanosecond decay of exciplex fluorescence.^{46–48} However, although powerful, this approach requires well-separated local and exciplex emission spectra.

Over the past years, time-resolved vibrational spectroscopy has proven to be the method of choice for obtaining deep structural insight into photoinduced processes.^{52–57} We have recently demonstrated how time-resolved infrared (TRIR) spectroscopy can be advantageously used to distinguish different intermediates involved in bimolecular photoinduced CS processes when no significant difference can be detected in the visible region.^{58–60} Tight ion pairs generated upon static quenching⁶¹ and loose ion pairs formed by dynamic quenching could be spectrally differentiated using the methylperylene/tetracyanoethylene (MePe/TCNE) D/A pair.⁵⁸ In a subsequent investigation with the cyanoanthracene/phthalic anhydride (CA/PA) pair in acetonitrile and tetrahydrofuran, distinct vibrational absorption bands associated with C=O and C≡N stretching modes of the exciplex could be clearly detected.⁵⁹ Analysis of the temporal evolution of the excited reactant, exciplex, and ion pair population over the first 2 ns after excitation revealed that the formation and recombination of the ion pairs in tetrahydrofuran is taking place almost exclusively via an exciplex. Because of the small CS driving force of this D/A pair, $\Delta G_{CS} \sim -0.1$ eV in acetonitrile, investigations in solvents less polar than tetrahydrofuran could not be carried out.

We report here on our investigation of bimolecular photoinduced CS with a D/A pair consisting of 9,10-dimethylantracene (DMeA) and 1,2-dicyanobenzene (phthalonitrile, PN) using TRIR spectroscopy in six solvents covering a broad range of polarity (Chart 1). For this, we used the highly polar solvents acetonitrile (ACN) and butyronitrile (BuCN), the medium polar solvents tetrahydrofuran (THF) and *n*-

propyl acetate (PrAc), and the weakly polar solvents *n*-butyl acetate (BuAc) and diethyl ether (Et₂O). Because of the better redox properties of the reactants compared to the CA/PA pair, CS is still energetically feasible in solvents as weak as Et₂O (Chart 1). Moreover, both DMeA and PN have good IR marker modes, such as the C=C and C≡N stretching vibrations. Our study reveals that static quenching results in the formation of a short-lived exciplex,⁶¹ whereas dynamic quenching leads to the parallel generation of a longer-lived exciplex and of an ion pair, with a ratio that depends on the solvent polarity. The herein obtained results will be compared with those from the above-mentioned D/A pairs (MePe/TCNE and CA/PA) to draw a comprehensive picture of the role of exciplexes in these reactions. We will also demonstrate how valuable information on the electronic density in a bimolecular complex can be deduced from the shape and position of absorption bands associated with specific vibrational modes.

EXPERIMENTAL SECTION

Chemicals. 9,10-Dimethylantracene (DMeA, Alfa Aesar, 99%) was used as received. Phthalonitrile (PN, Fluka, ~98%) was purified by sublimation before use. Acetonitrile (ACN, Fisher Scientific), butyronitrile (BuCN, Alfa Aesar), tetrahydrofuran (THF, Acros), *n*-propyl acetate (PrAc, Alfa Aesar), *n*-butyl acetate (BuAc, Acros), and diethyl ether (Et₂O, Sigma-Aldrich) were of the highest spectroscopic purity and used as received.

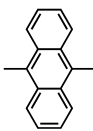
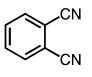
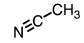
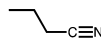
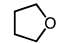
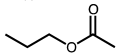
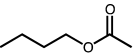
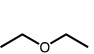
Steady-State Spectroscopy. Absorption spectra were recorded on a Cary 50 spectrophotometer, and the fluorescence spectra were measured on a Cary Eclipse fluorometer.

Time-Resolved Fluorescence. Subnanosecond time-resolved fluorescence dynamics were measured using the time-correlated single-photon counting (TCSPC) technique with the setup described in refs 62 and 63. Briefly, excitation was performed with a laser diode at 395 nm (Picoquant model LHD-P-C-400B). The pulse duration was 60 ps, and the full width at half-maximum (fwhm) of the instrument response function was about 200 ps. The emission was collected at magic angle after passing through an interference filter of 8 nm bandwidth at 450 nm. The absorbance of all sample solutions was <0.1 at the excitation wavelength in a 10 mm quartz cuvette.

Transient Electronic Absorption. Femtosecond transient electronic absorption spectra were recorded using the apparatus described in refs 64 and 65. The instrument response function had a fwhm of approximately 200 fs as obtained from measurements of the optical Kerr effect in ACN. The irradiance of the 400 nm excitation was about 0.5 mJ/cm². The sample absorbance at 400 nm was <0.3 in a 1 mm quartz cuvette. The samples were stirred with a Teflon rod during the experiment to constantly refresh the excitation volume, thus avoiding sample degradation. Absorbance changes of less than 7% were observed during an entire experiment. Each experiment is the average of six measurements obtained by scanning the translation stage back and forth three times.

Transient Vibrational Absorption. Femtosecond transient vibrational spectra were obtained with the setup described in ref 60 and 66. Excitation was performed with 0.6 μJ (0.6 mJ/cm²) pulses at 400 nm. The time-resolution of the experiment was around 300 fs as obtained from the absorption of a silicon wafer. The pulses were focused on the sample to a spot of 350 μm. Mid-IR probe pulses at around 4.7 μm (C≡N) and 7 μm

Chart 1. Electron Donor (Chromophore), Acceptor, and Solvents.^a

Donor	Acceptor	Solvents		
 DMeA	 PN	 ACN	 BuCN	 THF
		ϵ : 36	23	7.4
		$f(\epsilon)$: 0.96	0.94	0.81
		η : 0.36	0.57	0.46
		τ_f : 7.9	8.2	8.1
		ΔG_{CS} : -0.50	-0.45	-0.27
		 PrAc	 BuAc	 Et ₂ O
		ϵ : 6	5	4.3
		$f(\epsilon)$: 0.77	0.73	0.69
		η : 0.54	0.69	0.22
		τ_f : 7.4	7.8	7.4
		ΔG_{CS} : -0.20	-0.13	-0.07

^a ϵ , relative permittivity;⁴⁹ $f(\epsilon)$, Onsager polarity function; η , viscosity in cP;⁴⁹ τ_f , fluorescence lifetime of DMeA in ns; $-\Delta G_{CS}$, driving force of CS in eV calculated from the Weller equation (eq 16 in ref 50) with the redox potentials $E_{red}(PN) = -1.7$ V⁵¹ and $E_{ox}(DMeA) = 0.95$ V⁵¹ vs SCE, the excited-state energy $E_{00}(DMeA) = 3.08$ eV,⁵¹ ionic radii of 3.5 Å, and assuming contact.

(C=C) were generated by difference frequency mixing of the output of an optical parametric amplifier (Light Conversion, TOPAS-C with NDFG module). Detection was performed with a liquid nitrogen cooled 2×64 element MCT array (Infrared Systems Development), giving a resolution of $3\text{--}4\text{ cm}^{-1}$ (C \equiv N) and $1\text{--}2\text{ cm}^{-1}$ (C=C). The average of 3000 signal shots was taken to collect one data point with the polarization at magic angle. This procedure was carried out 20–30 times for each measurement and averaged. During each measurement, the sample was slightly moved vertically to hit different locations on the CaF₂ windows of the sample cell. To provide a new sample solution for each shot, a flow cell as described in ref 67 was used. The absorbance at 400 nm was around 0.22 on a 200 μm optical path length. No significant sample degradation was observed throughout the experiment. This was ensured by using a sufficiently large sample volume of up to 10 mL. No signal from solutions with PN only were obtained, and coherent effects due to the pump–probe overlap at zero time decayed within the first 200–300 fs in the pure solvents.

Quantum Chemistry Calculations. All the calculations were carried out at density functional theory (DFT) level in gas phase using the ADF package.^{68,69} The PBE functional was employed with the PEBx exchange correction and PBEC correlation term,⁷⁰ using a valence triple- ζ with one polarization function (TZP) as basis set.

RESULTS AND DISCUSSION

Steady-State and Time-Resolved Electronic Spectroscopy. Addition of PN to solutions of DMeA does not lead to any significant change in the $S_1 \leftarrow S_0$ absorption band of DMeA, and no new absorption feature associated with the formation of a D/A ground-state complex could be detected (Figure S1). The absence of a ground-state complex is consistent with the modest electron-donating and -accepting properties of D and A, respectively. As a consequence, excitation at 400 nm leads to the population of the locally excited state of DMeA only, even at high quenching concentration. On the other hand, addition of PN results in a decrease of DMeA fluorescence intensity and, in THF and lower polarity solvents, a broadening of the low-frequency side of the spectrum (Figure 1). Subtracting the DMeA fluorescence spectrum after proper normalization from the emission spectrum of DMeA/PN gives a broad red-shifted spectrum that can be assigned to an exciplex. In ACN and BuCN, the small difference in spectral shape cannot be attributed to an exciplex and is probably due to a nonspecific solvent effect. The presence of exciplex emission is consistent with the small driving force (Chart 1).

In the absence of quencher, the fluorescence dynamics of DMeA measured by time-correlated single-photon counting is monoexponential with a lifetime, τ_f , of the order of 8 ns (Chart 1, Figure S4). Upon addition of PN, the fluorescence decay is better described by a biexponential function with a fast component that accelerates with increasing quencher concentration and a slow component of low amplitude that has a 8–12 ns lifetime, independent of the PN concentration (Table S1). This biexponential behavior, which is more pronounced the lower the solvent polarity, is a typical indication of an equilibrium between the locally excited reactant and the quenching product that arises from the small energy gap between these two states.⁷¹ Although pure exciplex emission can be detected on the low-frequency side of the local

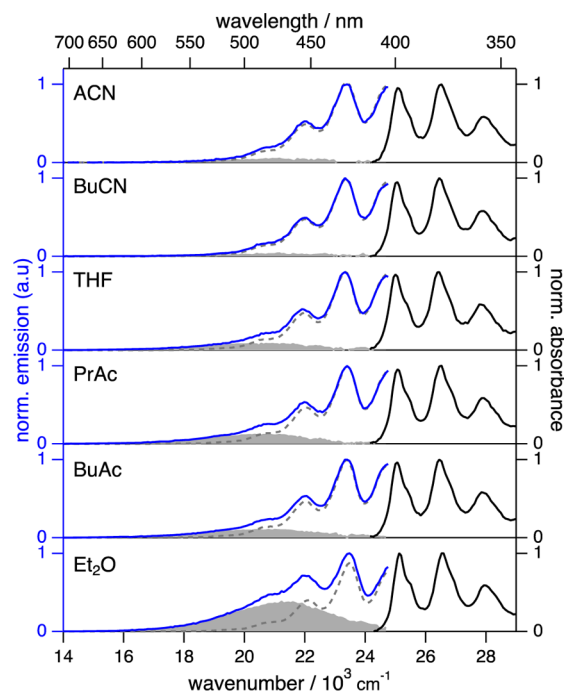


Figure 1. Normalized steady-state absorption (black) and emission spectra measured with DMeA and 0.05 M PN (blue) and with DMeA alone (dashed gray), and difference between the two spectra (filled gray).

fluorescence, its intensity is too small to yield reliable time profiles. This weak exciplex emission reflects the substantial charge-transfer character of the transition.⁷²

The Stern–Volmer analysis of the steady-state fluorescence intensity yields quenching rate constants that are comparable to the diffusion rate constant in ACN and BuCN, and smaller in the other less polar solvents (Figure S5 and Table S2). However, the Stern–Volmer analysis of the time-resolved fluorescence using only the faster decay component points to diffusion-controlled quenching except in Et₂O, where the quenching is slower (Table S2). The smaller quenching rate constants obtained from the steady-state emission intensity result from the equilibrium between the locally-excited reactant and the quenching product. Simulations of the fluorescence decays measured in Et₂O, where this effect is the strongest, using the Birk's excimer model^{71,73} confirmed that quenching is slower than diffusion (see Supporting Information).

Transient electronic absorption measurements confirm that fluorescence quenching originates from an electron transfer from DMeA in the S_1 state to PN. As illustrated in Figure 2, the transient spectra in ACN show the decrease of the $S_n \leftarrow S_1$ band at 585 nm and the parallel increase of bands at 655 and 420 nm arising from the DMeA radical cation, DMeA^{•+}.⁷⁴ The PN radical anion, PN^{•-}, does not absorb significantly between 400 and 750 nm and cannot be detected here.⁷⁴ Similar spectra could be observed in all solvents, the only difference being that the DMeA^{•+} bands are somewhat broader in the less polar solvents (Figure S6). However, no additional spectral feature that could be ascribed to an exciplex was detected.

TRIR Absorption Spectroscopy. Experiments were performed in the mid-IR in all six solvents, measuring first the vibrational response in the C \equiv N region between 2040 and 2160 cm^{-1} (Figure 3, left column). All measurements were performed with 0.4 M PN except those in BuAc (0.3 M) and in

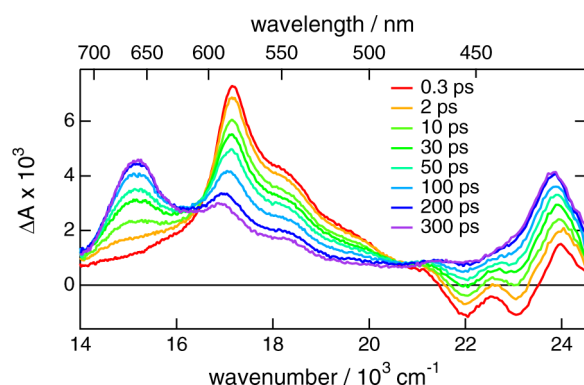


Figure 2. Transient electronic absorption spectra recorded at several time delays after 400 nm excitation of DMeA with 0.4 M PN in ACN.

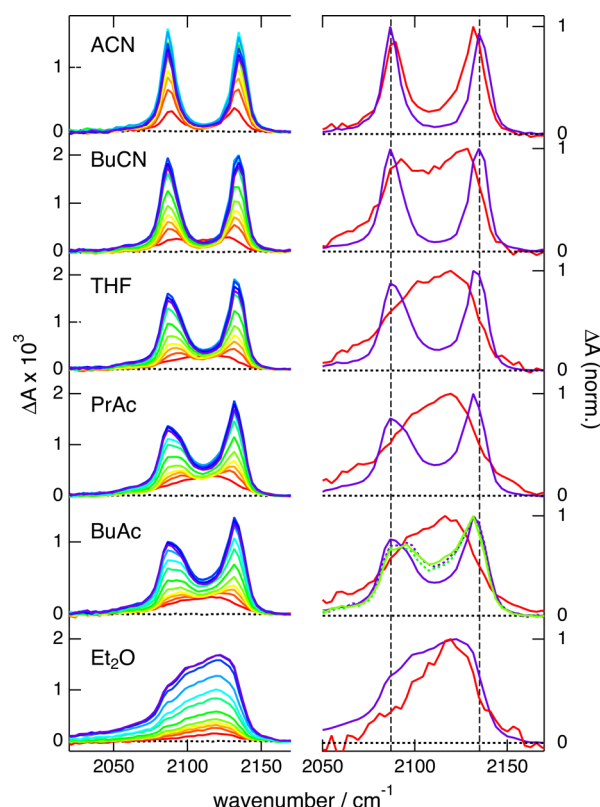


Figure 3. Left column: Transient IR absorption spectra associated with the antisymmetric $a[-C\equiv N]^{\bullet-}$ (2087 cm^{-1}) and symmetric $s[-C\equiv N]^{\bullet-}$ (2135 cm^{-1}) vibrations of the anion $PN^{\bullet-}$ and the $[-C\equiv N]^{\delta-}$ vibration of the exciplex (2113 cm^{-1}) measured with DMeA/PN after 400 nm excitation in various solvents. The concentration of PN was 0.4 M, except for BuAc (0.3 M) and Et_2O (0.05 M) (dashed line –30 ps; red to purple lines: 1, 10, 20, 30, 50, 100, 200, 300, 500, 1000, 1500, and 1900 ps). Right column: Corresponding intensity-normalized spectra at 1 ps (red) and 1900 ps (purple). Additionally, the normalized spectrum in BuAc at 100 ps (green) is compared with that recorded at 1900 ps with 0.05 M PN (dashed purple).

Et_2O (0.05 M) because of a lower solubility. Upon 400 nm excitation of an ACN solution, two positive absorption bands appear at 2087 and 2135 cm^{-1} . Their intensity increases continuously up to about 300 ps before starting to decay on a nanosecond time scale. During the first 10 ps, both bands undergo some narrowing, and the high-frequency one shifts to higher energy by about 3 cm^{-1} (Figure 3, right column). Both

bands can be reproduced by Lorentzian functions with a 10 cm^{-1} width (Figure S7). According to quantum chemical calculations, they can be attributed to the antisymmetric $a[-C\equiv N]^{\bullet-}$ (2087 cm^{-1}) and symmetric $s[-C\equiv N]^{\bullet-}$ (2135 cm^{-1}) stretching vibrations of the radical anion, $PN^{\bullet-}$ (Table S6).

A larger time-dependence of the band shape can be observed upon decreasing the solvent polarity. In THF and less polar solvents, the early spectra consist of a single broad band centered at 2113 cm^{-1} . With the exception of Et_2O , this band evolves into a spectrum with the two $[-C\equiv N]^{\bullet-}$ bands. However, the width of the $[-C\equiv N]^{\bullet-}$ bands as well as the signal intensity at the bottom of the dip between these bands (around 2113 cm^{-1}) become larger upon lowering the solvent polarity. Moreover, whereas the intensity ratio of both $[-C\equiv N]^{\bullet-}$ bands is around one in ACN and BuCN, the intensity of the high-frequency band increases relatively to that of the other band when going to less polar solvents. This spectral evolution is not seen in the lowest-polarity solvent Et_2O . Instead, the broad band observed at early time broadens further. However, this striking difference in Et_2O is not related to the lower quencher concentration (0.05 M). Transient spectra in BuCN and THF at 0.1 and 0.2 M PN and in BuAc at 0.05 M PN exhibit the same spectral evolution as that shown in Figure 3, but on a slower time scale, as expected (Figures S8 and S9). The origin of this broadening in Et_2O will be discussed in the next section.

The broad absorption feature observed at early time delay in BuCN and in the less polar solvents arises from the $-C\equiv N$ stretching mode of another transient species than $PN^{\bullet-}$, as the latter is characterized by two distinct bands located at lower and higher frequencies. The relative intensity of this broad band follows the same solvent dependence as the intensity of the exciplex fluorescence (Figure 1). Its shape and width are also very similar to those observed previously with the CA/PA exciplex.⁵⁹ Moreover, as discussed below, the position of this band coincides well with the $C\equiv N$ stretching frequencies calculated for the partially charged quencher $PN^{\delta-}$. Therefore, this band is attributed to a DMeA/PN exciplex, more specifically to the $[-C\equiv N]^{\delta-}$ stretching vibration of $PN^{\delta-}$ in the exciplex.

TRIR measurements were also performed in the $C=C$ stretch region between 1510 and 1610 cm^{-1} where only aromatic ring vibrations of DMeA are probed. Indeed, PN exhibits only weak absorption bands in this region (Figure S3), whereas the $[-C=C]^{\bullet-}$ aromatic ring vibrations of $PN^{\bullet-}$ are predicted to be at lower frequencies. In all six solvents, two positive bands, one at 1531 cm^{-1} and a less intense band at 1549 cm^{-1} , are visible at the earliest time delay (Figure 4, left column). As these bands decrease, a new band appears at 1589 cm^{-1} . The bands at 1531 and 1549 cm^{-1} are assigned to the $[-C=C]^*$ aromatic ring vibration of DMeA in the S_1 state, DMeA*, whereas the 1589 cm^{-1} band is attributed to the $[-C=C]^{\bullet+}$ aromatic ring vibration of DMeA*, in agreement with quantum chemistry calculations (Table S6) and with previous measurements on a similar anthracene derivative.⁵⁹

Compared to the spectra measured in the $C\equiv N$ region, substantial differences can be noticed (Figure 4): (i) The shape and position of the $[-C=C]^{\bullet+}$ band do not change with time and are the same in all six solvents. (ii) With the exception of ACN, no $[-C=C]^{\bullet+}$ band can be observed at early time delays, whereas a distinct band is already present in the $C\equiv N$ region.

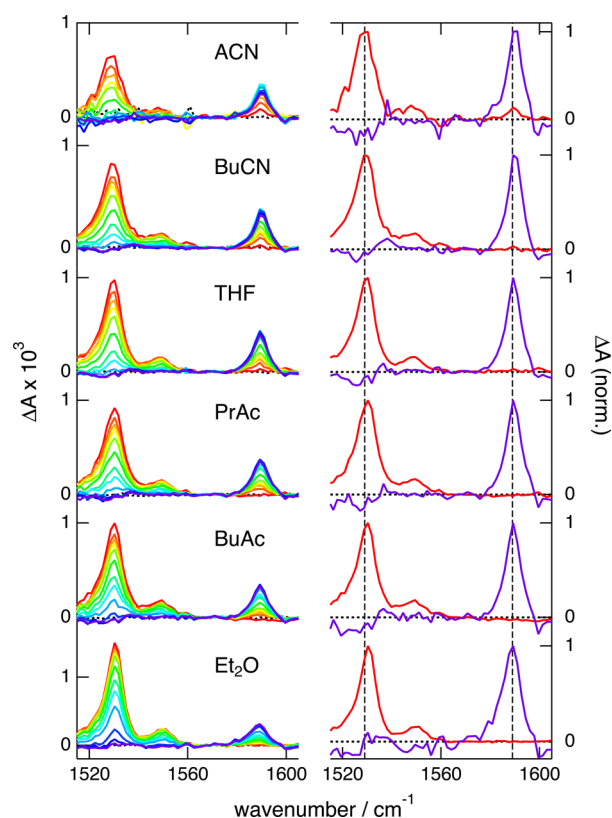


Figure 4. Left column: Transient IR spectra associated with the $[-C\equiv C-]^*$ (1531 and 1549 cm⁻¹) and $[-C\equiv C-]^{\bullet*}$ (1589 cm⁻¹) aromatic ring vibrations measured with DMeA/PN after excitation at 400 nm in six different solvents. The concentration of PN was 0.4 M, except for BuAc (0.3 M) and Et₂O (0.05 M) (dashed line –30 ps; red to purple lines: 1, 10, 20, 30, 50, 100, 200, 300, 500, 1000, 1500, and 1900 ps). Right column: Corresponding intensity-normalized spectra at 1 ps (red) and 1900 ps (purple).

Global Target Analysis. To obtain a deeper insight into the spectral evolution in both the C \equiv N and C=C regions, global target analysis of the IR transient spectra was performed assuming sequential first-order steps with increasing time constants.⁷⁵ In all solvents, five steps were required to properly reproduce the data, except in Et₂O where four steps were sufficient. The so-obtained time constants are listed in Table S3. Diffusion-controlled bimolecular photoinduced CS processes follow nonexponential dynamics.^{76–79} As a consequence, these time constants cannot be attributed to a given reaction step but only reflect a relevant time scale of the overall process. Similarly, the associated spectra cannot be assigned to a given species or state but are so-called evolution-associated difference spectra (EADS).⁷⁵

Contrary to what was assumed above from a superficial inspection of the transient spectra measured in the C \equiv N region (Figure 3), global target analysis reveals that the first EADS in ACN not only shows the two $[-C\equiv N]^{\bullet-}$ bands of the anion but also contains a contribution from the exciplex $[-C\equiv N]^{\delta-}$ band (Figure 5). In the other solvents, the first EADS exhibits only the exciplex band, additionally to the $[-C\equiv C-]^*$ band of DMeA*. This EADS transforms in 1–2 ps into the second one that, in the most polar solvents (ACN and BuCN), contains only the ion and DMeA* bands. The contribution from the exciplex has entirely decayed to zero in these two solvents. However, there is still no ion contribution

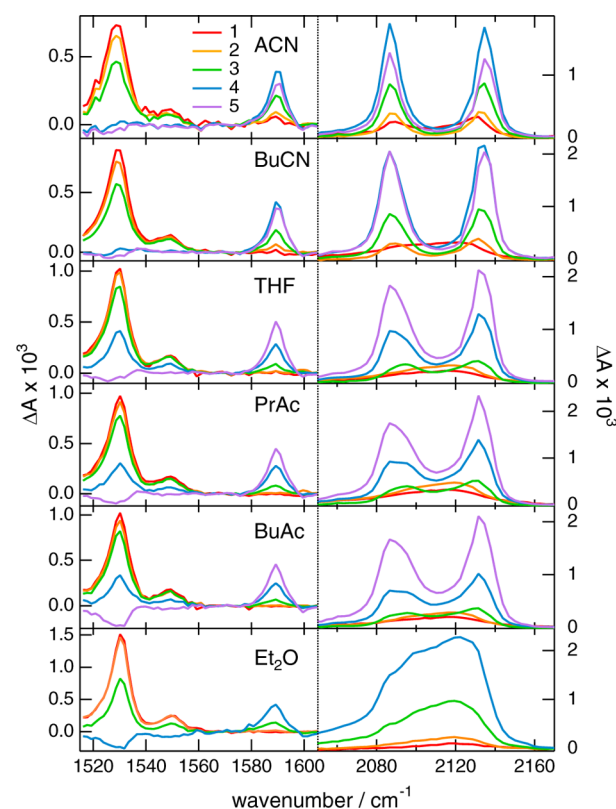


Figure 5. Evolution-associated difference spectra (EADS) obtained from global target analysis of the transient IR spectra assuming a series of successive steps with increasing time constants (the time constants are listed in Table S3).

in the other solvents, and only the exciplex is present in the C \equiv N region. Compared to the first EADS, the intensity of the exciplex band is noticeably larger, e.g., by a factor 1.5 in THF, whereas that of the DMeA* band remains almost constant. This observation will be discussed below.

In all solvents except Et₂O, this EADS evolves in ~10–20 ps to the third one that transforms in 100–200 ps into the fourth EADS, which itself converts in ~500 ps into the last. All three spectra exhibit the cation and anion bands. However, the presence of the exciplex $[-C\equiv N]^{\delta-}$ band remains also clearly visible in THF, PrAc, and BuAc. Indeed, subtraction of the rescaled exciplex spectrum (either the first or the second EADS) from these three EADS yields spectra that are very similar to those measured in ACN and due to the anion only (Figure S10). However, the differences from the ion spectra in ACN, already noticed in Figure 3 are still present: (i) the increase of bandwidth with decreasing solvent polarity is more pronounced with the low-frequency $^a[-C\equiv N]^{\bullet-}$ band, whose width increases from 10 cm⁻¹ in ACN to 14, 16, and 17 cm⁻¹ in THF, PrAc, and BuAc, respectively; (ii) the $^a[-C\equiv N]^{\bullet-}$ band is less intense than the other, whereas both $[-C\equiv N]^{\bullet-}$ bands have a similar intensity in ACN and BuCN.

Interestingly, the exciplex contribution in THF, PrAc, and BuAc decreases when going from the second to the third EADS and increases again in the fourth and fifth EADS. This suggests that exciplexes are involved during two different stages of the CS process. This will be confirmed below when inspecting the time profiles of the $[-C\equiv N]^{\delta-}$ band intensity.

In Et₂O, the third and fourth EADSs show the ion contribution in the C=C region. In the C \equiv N region, they

are still dominated by the exciplex band. In this latter region, these two EADSs are substantially broader than the first two. Subtraction of the first or second EADS from the fourth yields spectra with two bands at 2089 and 2130 cm^{-1} , which correspond to the $[-\text{C}\equiv\text{N}]^{\bullet-}$ stretching frequencies of $\text{PN}^{\bullet-}$ (Figure S10). Therefore, the broadening can be ascribed to the coexistence of exciplex and ions.

Kinetics and Reaction Mechanism. The temporal evolution of the intensity at the peak frequency of the DMeA^* , $\text{DMeA}^{\bullet+}$, $\text{PN}^{\bullet-}$, and exciplex bands is shown in Figure 6. Except in Et_2O , the decay of the DMeA^* population can be

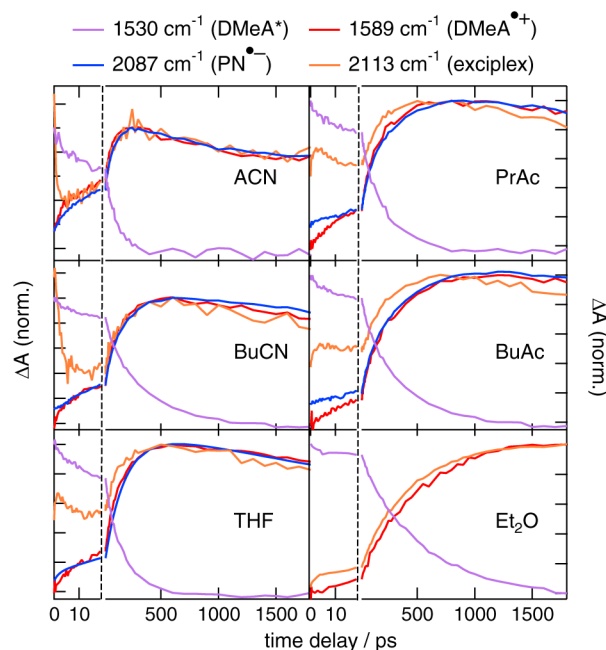


Figure 6. Intensity-normalized time profiles of the transient intensity at wavenumbers corresponding to the band maximum of the different intermediates. Note that in ACN, the time profiles of the exciplex may contain contribution of the anion. (The first 18 ps are represented using an enlarged time scale).

approximated by a biexponential function. Around 15–20% of the initial amplitude has an 8–24 ps lifetime, and the remaining amplitude has a lifetime ranging from 100 to 350 ps depending mostly on the solvent viscosity (Table S4). In Et_2O , the decay is slower because of the smaller quencher concentration and is almost exponential. Only 5% of the initial population decays with a 64 ps time constant, and the remainder has a 570 ps lifetime. Although a rigorous description of the quenching dynamics requires the use of an adequate model of diffusion-assisted reactions,^{76,80,81} which is beyond the scope of this study, the fast decay component reflects mostly the static and transient stages of the quenching, whereas the slow component is mainly associated with the stationary stage, the so-called dynamic quenching.

The time profiles of the $\text{DMeA}^{\bullet+}$ and $\text{PN}^{\bullet-}$ bands are identical within the limit of error of the measurements. The small difference that can be noticed within the first 20 ps in PrAc and BuAc probably arises from a small contribution of the exciplex band to the intensity at the $\text{PN}^{\bullet-}$ band maximum (2087 cm^{-1}). The ion profiles consist of a rise with a rate that increases with increasing solvent polarity followed by a slower decay that remains incomplete within the time window of the

experiment. Such comparison could not be done in Et_2O because of the strong overlap of the exciplex and anion bands. Deconvolution of the ion and exciplex contributions by band shape analysis proved to be unsuccessful because of too large a number of adjustable parameters.

As anticipated from the analysis of the EADS, the time profile of the 2113 cm^{-1} intensity reveals the presence of the exciplex at the earliest time delays in all solvents but Et_2O . In ACN and BuCN, the exciplex band decays almost entirely during the first few picoseconds, in agreement with the disappearance of the exciplex contribution observed when going from the first to the second EADS (Figure 5). The exciplex band then rises again, but to an intensity that is smaller than that at early time. From then on, it follows the same time dependence as that of the ion bands. Because of this similarity and the weakness of the signal, it can be suspected that this slower dynamics is in fact due to the ions and does not originate from the exciplex, at least in ACN. Indeed, no clear contribution of the exciplex to the second and next EADSs can be unambiguously established in ACN. In BuCN, the intensity in the region between the two $\text{PN}^{\bullet-}$ bands is larger than in ACN and could originate from the exciplex. In THF, PrAc, and BuAc, the initial exciplex intensity increases over the first 3–5 ps after excitation before decaying partially and rising again to reach a larger intensity than the initial one. Afterward, the intensity decays once more, but on a slower time scale. The second rise of the exciplex band is essentially identical to those of the ion bands (Table S5). The apparently faster increase of the exciplex band in THF and less polar solvents originates simply from a larger initial value. On the other hand, the following decay of the exciplex band is faster than those of the ion bands. In Et_2O , the exciplex intensity is initially very small and rises continuously up to 1.9 ns, the upper limit of the experiment.

The early and late formations of the exciplex could be related to the static and dynamics stages of the CS quenching, which are reflected by the nonexponential decay of the DMeA^* population. The presence of exciplex signal at the earliest time delay indicates that the quenching dynamics of DMeA^* has decay components that are too fast to be resolved in these measurements, where the first 300 fs were not taken into account in the analysis, because of the contribution of coherent effects to the transient signal.⁸² Because static quenching is favored at high quencher concentrations, the measurements in BuCN and THF were repeated at 0.1 and 0.2 M PN. The spectra in the $\text{C}\equiv\text{N}$ region obtained at these lower PN concentrations are very similar to those shown in Figure 3, the only difference being a slower spectral evolution (Figure S8). The time profiles of the exciplex intensity at different PN concentrations shown in Figure 7 reveal that the relative amplitude of the early exciplex population compared to that of the late exciplex decreases considerably with decreasing PN concentration, as expected for static quenching. For example, in THF, this relative amplitude changes from 0.66:1 at 0.4 M, 0.36:1 at 0.2 M, to 0.22:1 at 0.1 M PN. This decrease is accompanied by a slowing of the late exciplex population, in agreement with a formation by dynamic quenching.

These results reveal not only that the exciplex formation is bimodal but also that the early and late exciplexes are not identical as they are characterized by different lifetimes. This observation is analogous to that reported for the MePe/TCNE pair in ACN mentioned in the introduction.⁵⁸ There, the $[-\text{C}\equiv\text{N}]^{\bullet-}$ stretching bands of $\text{TCNE}^{\bullet-}$ produced by static quenching were found to be frequency shifted and to decay

loose exciplex and to the ion pair. In addition to recombination, the loose exciplex can “collapse” into a tight exciplex or evolve into an ion pair. The latter process should mostly involve solvation and some rotational and/or translational diffusion of the constituents. The ion pair itself can dissociate further into free ions on a time scale longer than that accessible in the experiment⁸⁵ and can in principle also transform into a loose exciplex. However, the slower decay of the ion pair signal compared to the loose exciplex signal requires the equilibrium between these two species to be on the ion pair side.

This scheme can also be used to rationalize the solvent dependence of the CS dynamics:

(1) In highly polar solvents (ACN and BuCN), the CS driving force is large enough for dynamic quenching to yield predominantly loose ion pairs. On the other hand, static quenching occurs with strongly coupled reactant pairs and results in tight exciplexes.

(2) In medium polar solvents (THF, PrAc, and BuAc), the CS driving force is smaller and relatively larger coupling is required to enable CS. Therefore, both loose exciplexes and ion pairs are formed upon dynamic quenching. Because of the weaker driving force, CS is no longer much faster than diffusion and static quenching becomes less important. Consequently, the tight exciplex population decreases with the solvent polarity, as illustrated in Figure 6.

(3) In the less polar Et₂O, CS is only slightly exergonic and is slower than diffusion. As a consequence, static quenching is hardly operative. As CS requires substantial coupling between the reactants to take place, almost only exciplexes are formed. In this case, the distinction between tight and loose exciplexes is probably no longer relevant.

In general, the product distribution due to dynamic quenching should narrow and shift toward exciplexes as the solvent polarity decreases, because quenching cannot take place unless coupling is large.

Exciplex Bandshape. The $[-C\equiv N]^{\delta-}$ stretching band of the exciplex is considerably broader than those of the ions in ACN, i.e., around 50 versus 10 cm⁻¹. Similarly broad absorption bands have been observed previously with the $[-C=O]^{\delta-}$ and $[-C\equiv N]^{\delta+}$ stretching modes of the CA/PA exciplex.⁵⁹ In principle, the bandwidth is directly related to the lifetime and dephasing time of the vibrational excited state. In the present case, it is difficult to justify a 5-fold acceleration of these processes upon going from the ions to the exciplex. As a consequence, this large bandwidth most probably arises from a distribution of mutual orientations and distances of the D and A moieties in the exciplex. This distribution is most certainly not static, but fluctuates during the lifetime of the exciplex. Orientation and distance should affect the overlap of the molecular orbitals of the constituents and influence the charge-transfer character of the exciplex. To explore the effect of a change of the electronic density in the D and A units on the frequency of the vibrational modes that are monitored in the TRIR measurements, quantum chemistry calculations at the DFT level have been carried out. In the case of PN^{•-}, these calculations predict the antisymmetric and symmetric $[-C\equiv N]^{\bullet-}$ stretching modes at 2099 and 2141 cm⁻¹, in good agreement with the experimental values of 2087 and 2135 cm⁻¹ (Table S6). For the neutral PN, a single absorption band is measured at 2233 cm⁻¹ (Figure S3), whereas the antisymmetric and symmetric $-C\equiv N$ stretching modes are calculated to be at 2246 and 2242 cm⁻¹. This shows that not only the frequencies but also the frequency difference between

the antisymmetric and symmetric modes, $\Delta\tilde{\nu}_{CN}$, are very sensitive to the electronic density on PN. To explore this effect further, the frequencies of these two modes were calculated while continuously decreasing the charge on PN from -1 to 0. Figure 9 reveals that $\Delta\tilde{\nu}_{CN}$ is slightly negative for the neutral

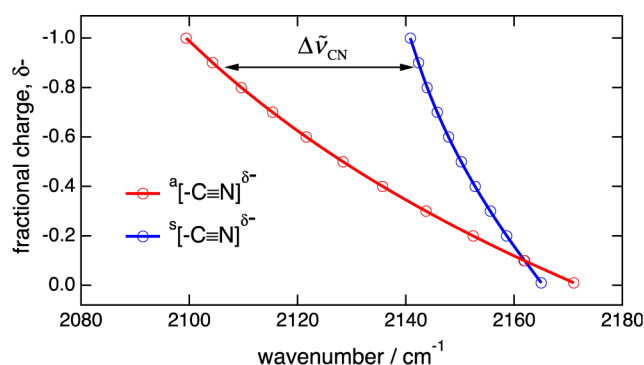


Figure 9. Calculated dependence of the asymmetric and symmetric $[-C\equiv N]^{\delta-}$ stretching frequencies of PN on the fractional charge δ^- (the continuous lines are only guides to the eye).

PN, zero at a partial charge of -0.1, and increases to about 42 cm⁻¹ for the anion. These calculations also indicate that the intensity of both bands increases considerably with increasing negative charge (Figure S11), in agreement with the negligibly small $-C\equiv N$ bleach signal of PN around 2230 cm⁻¹. Moreover, the intensity ratio between the antisymmetric and symmetric bands is predicted to be slightly above 1 for PN^{•-} and to decrease to about 0.4 for PN (Figure S12). This result agrees qualitatively well with the experiment, as illustrated in Figure 3.

In the case of DMeA^{•+}, bands at 1527 and 1576 cm⁻¹ are calculated (Table S6), whereas only one band is experimentally observed at 1589 cm⁻¹ (Figure 4). The lower-frequency band is predicted to shift by only -4 cm⁻¹ upon going from DMeA^{•+} to DMeA. Because of this small shift, the negative signal due to the bleach of DMeA and the positive band of DMeA^{•+} overlap and cancel out. Therefore, no transient band can be detected at this frequency (Figure 4, right column) once the band due to the $[-C=C-]^*$ vibration of DMeA^{*}, which is also located here, has entirely decayed. The similar $-C=C-$ stretching frequencies of DMeA, DMeA^{*}, and DMeA^{•+} could explain why the 1531 cm⁻¹ band remains almost unchanged when going from the first to the second EADS in THF, PrAc, and BuAc, whereas the exciplex band increases markedly (Figure 5).

A larger shift is predicted for the higher-frequency $-C=C-$ stretching mode, and indeed, bands at 1590 and 1620 cm⁻¹ are experimentally observed for DMeA^{•+} and DMeA (Figure S3), respectively. However, this ~30 cm⁻¹ frequency shift remains much smaller than those observed with the $-C\equiv N$ vibrations, especially that of 146 cm⁻¹ measured with the asymmetric mode. Furthermore, the intensity of the $[-C=C-]^{\bullet+}$ band is much smaller than that of the $[-C\equiv N]^{\bullet-}$ bands; therefore, the $[-C=C-]^{\delta+}$ exciplex band may simply be too weak to be visible.

These calculations fully support the existence of a distribution of exciplex geometry, hence of electronic coupling and charge-transfer character, as the origin of the anomalously large width of the $[-C\equiv N]^{\delta-}$ stretching band. Because of the large overlap of the exciplex and ion pair bands, spectral differences between the tight and loose exciplexes cannot be

detected. However, their existence is firmly supported by the time evolution of the band intensity. The increasing width of the $[-C\equiv N]^{\delta-}$ bands and the change of their relative intensity observed upon going from ACN to less polar solvents probably also reflect a distribution of the ion pair geometries with different coupling and a gradual shift toward the exciplex.

The ability of TRIR to detect exciplexes depends very much on the vibrational mode that is monitored. For the pair studied here, an exciplex band is only visible with the $[-C\equiv N]^{\delta-}$ stretching mode of the acceptor. In our previous investigation with the CA/PA pair,⁵⁹ exciplex features were observed with both donor and acceptor modes, $[-C\equiv N]^{\delta+}$ and $[-C=O]^{\delta-}$ stretching, respectively. However, the relative intensity of the donor band was much weaker than that of the acceptor band. In that case as well, no band associated with the $[-C=C-]^{\delta+}$ mode of the donor could be detected. This suggests that the observation of exciplex bands requires IR marker modes with at least two properties: (1) a larger absorption coefficient in the ionic than in the neutral forms and (2) a large frequency difference between the ionic and neutral forms. The $-C=O$ and $-C\equiv N$ stretching modes fulfill both conditions when located on the acceptor, i.e., when the charge varies from 0 to -1 . When located on the donor, their absorption coefficient decreases considerably upon going from the neutral to the cationic forms. In the case of the aromatic $-C=C-$ stretching modes, the first condition is often fulfilled but the second is generally not satisfied. This can be explained by the small change of C–C bond order brought about by the addition or the removal of an electron to an aromatic hydrocarbon as extended as anthracene. For the same reason, the $-C=O$ and $-C\equiv N$ vibration frequencies change more upon addition of an electron when located on a small π -conjugated system, such as ethylene or benzene, than when present on a larger aromatic molecule like anthracene.

CONCLUSIONS AND OUTLOOK

This investigation is a further demonstration of the strength of TRIR spectroscopy for unraveling the details of bimolecular photoinduced charge separation processes. By investigating a D/A pair with a moderate driving force for electron transfer in solvents with a broad range of polarity, a deeper insight into the role of exciplexes was obtained. By monitoring the temporal evolution of the locally excited reactants, ions, and exciplex via their distinctive spectral features, we could evidence the existence of two forms of exciplexes: short-lived, tight, exciplexes generated upon static quenching and longer-lived, loose, exciplexes formed together with loose ion pairs upon dynamic quenching. Similarly to the ion pairs, these tight and loose exciplexes correspond to two limits of a broad distribution of exciplexes with different geometry, electronic coupling, and charge-transfer character, as indicated by the anomalously large IR bandwidth. All these intermediates differ mostly by the magnitude of the electronic coupling and charge-transfer character.

The quenching product distribution depends on the driving force, which is itself influenced by the solvent polarity. The weaker the driving force, the higher the electronic coupling required for making charge separation feasible. Similarly, at small driving force, quenching is slower than diffusion and is thus purely dynamic. On the other hand, as soon as the intrinsic charge separation rate constant is larger than that of diffusion, static quenching is also operative. This is the case here in highly polar solvents, where static and dynamic quenching yield tight

exciplexes and loose ion pairs, respectively. In medium polarity solvents, dynamic quenching generates loose exciplexes as well. Finally, in weakly polar solvents, the quenching is entirely dynamic and results predominantly in exciplexes.

This study complements two previous TRIR investigations performed with D/A pairs characterized by lower and higher driving forces.^{58,59} In the first case, the product of the quenching, which was purely dynamic, was found to be an exciplex and to be the precursor of ion pairs.⁵⁹ In the second case, no exciplex but two ion pair-like transients were detected: a short-lived tight ion pair generated upon static quenching and a longer-lived loose ion pair formed upon dynamic quenching.⁵⁸

The present investigation was focused on the nature of the primary quenching product. This knowledge is of crucial importance for many applications in which free ions or charge carriers have to be generated with high efficiency. The temporal evolution of these various intermediates on a longer time scale is being presently investigated and will be discussed in detail in a forthcoming paper.

The high sensitivity of the vibrational frequency of specific marker modes to the electronic density could be exploited in the future as a local probe of the extent of charge transfer in other D/A systems, where full charge separation is often assumed from the observation of ion bands in transient electronic absorption spectra. This approach should be especially fruitful for rigid D–A dyads for which the band broadening due to the conformational distribution is eliminated.

ASSOCIATED CONTENT

Supporting Information

The Supporting Information is available free of charge on the ACS Publications website at DOI: 10.1021/acs.jpcb.5b07663.

Additional experimental details, fluorescence quenching, time-resolved fluorescence, transient electronic and infrared absorption spectra, data analysis, and quantum chemistry calculations (PDF)

AUTHOR INFORMATION

Corresponding Author

*E-mail: eric.vauthey@unige.ch.

Present Address

[†]M.K.: Department of Chemistry, Princeton University, NJ.

Notes

The authors declare no competing financial interest.

ACKNOWLEDGMENTS

The work was supported by the Fonds National Suisse de la Recherche Scientifique through project no 200020-147098 and by the University of Geneva.

REFERENCES

- (1) Leonhardt, H.; Weller, A. Elektronenuebertragungsreaktionen des Angeregten Perylens. *Ber. Bunsenges. Phys. Chem.* **1963**, *67*, 791–795.
- (2) Weller, A. Exciplex and Radical Pairs in Photochemical Electron Transfer. *Pure Appl. Chem.* **1982**, *54*, 1885–1888.
- (3) Mataga, N.; Miyasaka, H. Electron Transfer and Exciplex Chemistry. *Adv. Chem. Phys.* **1999**, *107*, 431–496.

- (4) Brouwer, F. Structural Aspects of Exciplex Formation. In *Conformational Analysis of Molecules in Excited States*; Waluk, J., Ed.; Wiley-VCH: New York, 2000; p 177.
- (5) Mataga, N.; Chosrowjan, H.; Taniguchi, S. Ultrafast Charge Transfer in Excited Electronic States and Investigations into Fundamental Problems of Exciplex Chemistry: Our Early Studies and Recent Developments. *J. Photochem. Photobiol., C* **2005**, *6*, 37–79.
- (6) Swinnen, A. M.; Van der Auweraer, M.; de Schryver, F. C.; Nakatani, K.; Okada, T.; Mataga, N. Photophysics of the Intramolecular Exciplex Formation in *w*-(1-pyrenyl)- α -N,N-dimethylaminoalkanes. *J. Am. Chem. Soc.* **1987**, *109*, 321–330.
- (7) Wasielewski, M. R.; Minsek, D. V.; Niemczyk, M. P.; Svec, W. A.; Yang, N. Intramolecular Light-Induced Electron Transfer in a Rigid, Fixed-Distance Anthracene-N,N-Dimethylaniline System. Exciplex-like Behavior. *J. Am. Chem. Soc.* **1990**, *112*, 2823–2824.
- (8) Mataga, N.; Nishikawa, S.; Asahi, T.; Okada, T. Femtosecond-Picosecond Laser Photolysis Studies on the Photoinduced Charge Separation and Charge Recombination of a Produced Ion Pair State of some Typical Intramolecular Exciplex Compounds in Alkanenitrile Solvents. *J. Phys. Chem.* **1990**, *94*, 1443–1447.
- (9) Banerji, N.; Angulo, G.; Barabanov, I. I.; Vauthey, E. Intramolecular Charge-Transfer Dynamics in Covalently Linked Perylene-Dimethylaniline and Cyanoperylene-Dimethylaniline. *J. Phys. Chem. A* **2008**, *112*, 9665–9674.
- (10) Al Subi, A. H. A.; Niemi, M. M.; Tkachenko, N. V. N.; Lemmetyinen, H. H. Quantitative Analysis of Intramolecular Exciplex and Electron Transfer in a Double-Linked Zinc Porphyrin-Fullerene Dyad. *J. Phys. Chem. A* **2012**, *116*, 9653–9661.
- (11) Nakashima, N.; Mataga, N.; Ushio, F.; Yamanaka, C. Time-Resolved Fluorescence Studies on Exciplexes. *Z. Phys. Chem.* **1972**, *79*, 150–167.
- (12) Palmans, J. P.; Van der Auweraer, M.; Swinnen, A.; De Schryver, F. C. Intermolecular Exciplex Formation between Pyrene Derivatives and 1,2-Dimethylindole. *J. Am. Chem. Soc.* **1984**, *106*, 7721–7728.
- (13) Kikuchi, K.; Niwa, T.; Takahashi, Y.; Ikeda, H.; Miyashi, T.; Hoshi, M. Evidence of Exciplex Formation in Acetonitrile. *Chem. Phys. Lett.* **1990**, *173*, 421–424.
- (14) Gould, I. R.; Young, R. H.; Mueller, L. J.; Farid, S. Mechanism of Exciplex formation. Role of Superexchange, Solvent Polarity, and Driving Force for Electron Transfer. *J. Am. Chem. Soc.* **1994**, *116*, 8176–8187.
- (15) Iwai, S.; Murata, S.; Katoh, R.; Tachiya, M.; Kikuchi, K.; Takahashi, Y. Ultrafast Charge Separation and Exciplex Formation Induced by Strong Interaction between Electron Donor and Acceptor at Short Distances. *J. Chem. Phys.* **2000**, *112*, 7111–7117.
- (16) Kuzmin, M. G. M.; Soboleva, I. V. I.; Dolotova, E. V. E.; Dogadkin, D. N. D. Evidence for Diffusion-Controlled Electron Transfer in Exciplex Formation Reactions. Medium Reorganisation Stimulated by Strong Electronic Coupling. *Photochem. Photobiol. Sci.* **2003**, *2*, 967–974.
- (17) Morandeira, A.; Fürstenberg, A.; Vauthey, E. Fluorescence Quenching in Electron Donating Solvents. 2. Solvent Dependence and Product Dynamics. *J. Phys. Chem. A* **2004**, *108*, 8190–8200.
- (18) Morteaux, A. C. A.; Sreearunothai, P. P.; Herz, L. M. L.; Friend, R. H. R.; Silva, C. C. Exciton Regeneration at Polymeric Semiconductor Heterojunctions. *Phys. Rev. Lett.* **2004**, *92*, 247402.
- (19) Offermans, T.; van Hal, P. A.; Meskers, S. S.; Koetse, M. S.; Janssen, R. R. Exciplex Dynamics in a Blend of π -Conjugated Polymers with Electron Donating and Accepting Properties: MDMO-PPV and PCNEPV. *Phys. Rev. B: Condens. Matter Mater. Phys.* **2005**, *72*, 045213.
- (20) Benson Smith, J. J.; Wilson, J. J.; Dyer Smith, C. C.; Mouri, K. K.; Yamaguchi, S. S.; Murata, H. H.; Nelson, J. J. Long-Lived Exciplex Formation and Delayed Exciton Emission in Bulk Heterojunction Blends of Silole Derivative and Polyfluorene Copolymer: the Role of Morphology on Exciplex Formation and Charge Separation. *J. Phys. Chem. B* **2009**, *113*, 7794–7799.
- (21) Dyer-Smith, C. C.; Benson-Smith, J. J.; Bradley, D. D. C.; Murata, H.; Mitchell, W. J.; Shaheen, S. E.; Haque, S. A.; Nelson, J. The Effect of Ionization Potential and Film Morphology on Exciplex Formation and Charge Generation in Blends of Polyfluorene Polymers and Silole Derivatives. *J. Phys. Chem. C* **2009**, *113*, 14533–14539.
- (22) Shepherd, W. E. B.; Platt, A. D. A.; Kendrick, M. J. M.; Loth, M. A. M.; Anthony, J. E. J.; Ostroverkhova, O. O. Energy Transfer and Exciplex Formation and Their Impact on Exciton and Charge Carrier Dynamics in Organic Films. *J. Phys. Chem. Lett.* **2011**, *2*, 362–366.
- (23) Stewart, D. J. D.; Dalton, M. J. M.; Swiger, R. N. R.; Cooper, T. M. T.; Haley, J. E. J.; Tan, L. L.-S. Exciplex Formation in Blended Spin-Cast Films of Fluorene-Linked Dyes and Bisphthalimide Quenchers. *J. Phys. Chem. A* **2013**, *117*, 3909–3917.
- (24) Chao, C. I.; Chen, S. A. White Light Emission from Exciplex in a Bilayer Device with Two Blue Light-Emitting Polymers. *Appl. Phys. Lett.* **1998**, *73*, 426–428.
- (25) Feng, J.; Li, F.; Gao, W. B.; Liu, S. Y.; Wang, Y. White Light Emission from Exciplex Using Tris-(8-hydroxyquinoline)aluminum as Chromaticity-Tuning Layer. *Appl. Phys. Lett.* **2001**, *78*, 3947–3949.
- (26) Morteaux, A. C.; Friend, R. H.; Silva, C. Endothermic Exciplex-Exciton Energy-Transfer in a Blue-Emitting Polymeric Heterojunction System. *Chem. Phys. Lett.* **2004**, *391*, 81–84.
- (27) Kim, J.-S.; Lu, L.; Sreearunothai, P.; Seeley, A.; Yim, K.-H.; Petrozza, A.; Murphy, C. E.; Beljonne, D.; Cornil, J.; Friend, R. H. Optoelectronic and Charge Transport Properties at Organic–Organic Semiconductor Interfaces: Comparison between Polyfluorene-Based Polymer Blend and Copolymer. *J. Am. Chem. Soc.* **2008**, *130*, 13120–13131.
- (28) Goushi, K.; Yoshida, K.; Sato, K.; Adachi, C. Organic Light-Emitting Diodes Employing Efficient Reverse Intersystem Crossing for Triplet-to-Singlet State Conversion. *Nat. Photonics* **2012**, *6*, 253–258.
- (29) Crespo-Hernandez, C. E.; Cohen, B.; Hare, P. M.; Kohler, B. Ultrafast Excited-State Dynamics in Nucleic Acids. *Chem. Rev.* **2004**, *104*, 1977–2019.
- (30) Markovitsi, D.; Talbot, F.; Gustavsson, T.; Onidas, D.; Lazzarotto, E.; Marguet, S. Molecular spectroscopy: Complexity of excited-state dynamics in DNA. *Nature* **2006**, *441*, E7.
- (31) Takaya, T.; Su, C.; de La Harpe, K.; Crespo-Hernández, C. E.; Kohler, B. UV Excitation of Single DNA and RNA Strands Produces High Yields of Exciplex States between Two Stacked Bases. *Proc. Natl. Acad. Sci. U. S. A.* **2008**, *105*, 10285–10290.
- (32) Doorley, G. W.; Wojdyla, M.; Watson, G. W.; Towrie, M.; Parker, A. W.; Kelly, J. M.; Quinn, S. J. Tracking DNA Excited States by Picosecond-Time-Resolved Infrared Spectroscopy: Signature Band for a Charge Transfer Excited State in Stacked Adenine-Thymine Systems. *J. Phys. Chem. Lett.* **2013**, *4*, 2739–2744.
- (33) Romero, E. E.; Diner, B. A. B.; Nixon, P. J. P.; Coleman, W. J. W.; Dekker, J. P. J.; van Grondelle, R. R. Mixed Exciton-Charge-Transfer States in Photosystem II: Stark Spectroscopy on Site-Directed Mutants. *Biophys. J.* **2012**, *103*, 185–194.
- (34) Brunschwig, B. S.; Ehrenson, S.; Sutin, N. Distance Dependence of Electron Transfer Reactions: Rate Maxima and Rapid Rates at Large Separations. *J. Am. Chem. Soc.* **1984**, *106*, 6858–6859.
- (35) Kakitani, T.; Yoshimori, A.; Mataga, N. Effects of the Donor-Acceptor Distance Distribution on the Energy Gap Laws of Charge Separation and Charge Recombination Reactions in Polar Solutions. *J. Phys. Chem.* **1992**, *96*, 5385–5392.
- (36) Murata, S.; Tachiya, M. Transient Effect in Fluorescence Quenching by Electron Transfer. 3. Distribution of Electron Transfer Distance in Liquid and Solid Solutions. *J. Phys. Chem.* **1996**, *100*, 4064–4070.
- (37) Vauthey, E. Investigations of Bimolecular Photoinduced Electron Transfer Reactions in Polar Solvents using Ultrafast Spectroscopy. *J. Photochem. Photobiol., A* **2006**, *179*, 1–12.
- (38) Rosspeintner, A.; Kattnig, D. R.; Angulo, G.; Landgraf, S.; Grampp, G. The Rehm–Weller Experiment in View of Distant Electron Transfer. *Chem. - Eur. J.* **2008**, *14*, 6213–6221.
- (39) Kamat, P. V. P. Meeting the Clean Energy Demand: Nanostructure Architectures for Solar Energy Conversion. *J. Phys. Chem. C* **2007**, *111*, 2834–2860.

- (40) Heeger, A. J. A. Semiconducting Polymers: the Third Generation. *Chem. Soc. Rev.* **2010**, 39, 2354–2371.
- (41) Clarke, T. M.; Durrant, J. R. Charge Photogeneration in Organic Solar Cells. *Chem. Rev.* **2010**, 110, 6736–6767.
- (42) Silva, C. Organic Photovoltaics: Some Like it Hot. *Nat. Mater.* **2013**, 12, 5–6.
- (43) Ottolenghi, M. Charge Transfer Complexes in the Excited State. *Laser Photolysis Studies. Acc. Chem. Res.* **1973**, 6, 153–160.
- (44) Okada, T.; Migita, M.; Mataga, N.; Sakata, Y.; Misumi, S. Picosecond Laser Spectroscopy of Intramolecular Heteroexcimer Systems. Time-Resolved Absorption Studies of p-(CH₃NC₆H₄-(CH₂))₁ -pyrenyl and -(9-anthryl) Systems. *J. Am. Chem. Soc.* **1981**, 103, 4715–4720.
- (45) Vauthey, E.; Högemann, C.; Allonas, X. Direct Investigation of the Dynamics of Charge Recombination Following the Fluorescence Quenching of 9,10-Dicyanoanthracene by Various Electron Donors in Acetonitrile. *J. Phys. Chem. A* **1998**, 102, 7362–7369.
- (46) Kattnig, D. R.; Rosspeintner, A.; Grampp, G. Magnetic Field Effects on Exciplex-Forming Systems: the Effect on the Locally Excited Fluorophore and its Dependence on Free Energy. *Phys. Chem. Chem. Phys.* **2011**, 13, 3446–3460.
- (47) Richert, S.; Rosspeintner, A.; Landgraf, S.; Grampp, G.; Vauthey, E.; Kattnig, D. R. Time-Resolved Magnetic Field Effects Distinguish Loose Ion Pairs from Exciplexes. *J. Am. Chem. Soc.* **2013**, 135, 15144–15152.
- (48) Hoang, H. M.; Pham, T. B. V.; Grampp, G.; Kattnig, D. R. Exciplexes versus Loose Ion Pairs: How Does the Driving Force Impact the Initial Product Ratio of Photoinduced Charge Separation Reactions? *J. Phys. Chem. Lett.* **2014**, 5, 3188–3194.
- (49) Riddick, J. A.; Bunger, W. B. *Organic Solvents*. J. Wiley: New York, 1970.
- (50) Weller, A. Photoinduced Electron Transfer in Solutions: Exciplex and Radical Ion Pair Formation Free Enthalpies and their Solvent Dependence. *Z. Phys. Chem.* **1982**, 133, 93–98.
- (51) Montalti, M.; Credi, A.; Prodi, L.; Gandolfi, M. T. *Handbook of Photochemistry*, 3rd ed.; Taylor & Francis: Boca Raton, FL, 2006.
- (52) Nibbering, E. T. J.; Fidler, H.; Pines, E. Ultrafast Chemistry: Using Time-Resolved Vibrational Spectroscopy for Interrogation of Structural Dynamics. *Annu. Rev. Phys. Chem.* **2005**, 56, 337–367.
- (53) Olofsson, J.; Onfelt, B.; Lincoln, P.; Norden, B.; Matousek, P.; Parker, A. W.; Tuite, E. Picosecond Kerr-Gated Time-Resolved Resonance Raman Spectroscopy of the [Ru(phen)₂dppz]²⁺ Interaction with DNA. *J. Inorg. Biochem.* **2002**, 91, 286–297.
- (54) Kukura, P.; McCamant, D. W.; Yoon, S.; Wandschneider, D. B.; Mathies, R. A. Structural Observation of the Primary Isomerization in Vision with Femtosecond-Stimulated Raman. *Science* **2005**, 310, 1006–1009.
- (55) Weigel, A.; Dobryakov, A.; Klaumünzer, B.; Sajadi, M.; Saalfrank, P.; Ernsting, N. P. Femtosecond Stimulated Raman Spectroscopy of Flavins after Optical Excitation. *J. Phys. Chem. B* **2011**, 115, 3656–3680.
- (56) Zhang, Y.; Dood, J.; Beckstead, A. A.; Li, X.-B.; Nguyen, K. V.; Burrows, C. J.; Improt, R.; Kohler, B. Efficient UV-Induced Charge Separation and Recombination in an 8-Oxoguanine-Containing Dinucleotide. *Proc. Natl. Acad. Sci. U. S. A.* **2014**, 111, 11612–11617.
- (57) Provencher, F.; Bérubé, N.; Parker, A. W.; Greetham, G. M.; Towrie, M.; Hellmann, C.; Côté, M.; Stingelin, N.; Silva, C.; Hayes, S. C. Direct Observation of Ultrafast Long-Range Charge Separation at Polymer–Fullerene Heterojunctions. *Nat. Commun.* **2014**, 5, DOI: 10.1038/ncomms5288
- (58) Mohammed, O. F.; Adamczyk, K.; Banerji, N.; Dreyer, J.; Lang, B.; Nibbering, E. T. J.; Vauthey, E. Direct Femtosecond Observation of Tight and Loose Ion Pairs upon Photoinduced Bimolecular Electron Transfer. *Angew. Chem., Int. Ed.* **2008**, 47, 9044–9048.
- (59) Koch, M.; Letrun, R.; Vauthey, E. Exciplex Formation in Bimolecular Photoinduced Electron-Transfer Investigated by Ultrafast Time-Resolved Infrared Spectroscopy. *J. Am. Chem. Soc.* **2014**, 136, 4066–4074.
- (60) Koch, M.; Rosspeintner, A.; Adamczyk, K.; Lang, B.; Dreyer, J.; Nibbering, E. T. J.; Vauthey, E. Real-Time Observation of the Formation of Excited Radical Ions in Bimolecular Photoinduced Charge Separation: Absence of the Marcus Inverted Region Explained. *J. Am. Chem. Soc.* **2013**, 135, 9843–9848.
- (61) By static quenching, we mean a process in which the reactants do not have to diffuse as they are already at optimal distance and orientation. Static quenching is not due to the direct excitation in the charge-transfer band of a ground-state complex.
- (62) Muller, P.-A.; Högemann, C.; Allonas, X.; Jacques, P.; Vauthey, E. Deuterium Isotope Effect on the Charge Recombination Dynamics of Contact Ion Pairs Formed by Electron Transfer Quenching in Acetonitrile. *Chem. Phys. Lett.* **2000**, 326, 321–327.
- (63) Fürstenberg, A.; Vauthey, E. Excited State Dynamics of the Fluorescent Probe Lucifer Yellow in Liquid Solutions in Heterogeneous Media. *Photochem. Photobiol. Sci.* **2005**, 4, 260–267.
- (64) Duvanel, G.; Banerji, N.; Vauthey, E. Excited-State Dynamics of Donor-Acceptor Bridged Systems Containing a Boron-Dipyrromethene Chromophore: Interplay between Charge Separation and Reorientational Motion. *J. Phys. Chem. A* **2007**, 111, 5361–5369.
- (65) Banerji, N.; Duvanel, G.; Perez-Velasco, A.; Maity, S.; Sakai, N.; Matile, S.; Vauthey, E. Excited-State Dynamics of Hybrid Multichromophoric Systems: Toward an Excitation Wavelength Control of the Charge Separation Pathways. *J. Phys. Chem. A* **2009**, 113, 8202–8212.
- (66) Letrun, R.; Koch, M.; Dekhtyar, M. L.; Kurdyukov, V. V.; Tolmachev, A. I.; Rettig, W.; Vauthey, E. Ultrafast Excited-State Dynamics of Donor–Acceptor Biaryls: Comparison between Pyridinium and Pyrilyum Phenolates. *J. Phys. Chem. A* **2013**, 117, 13112–13126.
- (67) Bredenbeck, J.; Hamm, P. Versatile Small Volume Closed-Cycle Flow Cell System for Transient Spectroscopy at High Repetition Rates. *Rev. Sci. Instrum.* **2003**, 74, 3188–3189.
- (68) Fonseca Guerra, C.; Snijders, J. G.; te Velde, G.; Baerends, E. J. Towards an order- N DFT method. *Theor. Chem. Acc.* **1998**, 99, 391–403.
- (69) te Velde, G.; Bickelhaupt, F. M.; Baerends, E. J.; Fonseca Guerra, C.; van Gisbergen, S. J. A.; Snijders, J. G.; Ziegler, T. Chemistry with ADF. *J. Comput. Chem.* **2001**, 22, 931–967.
- (70) Perdew, J. P.; Burke, K.; Ernzerhof, M. Generalized Gradient Approximation Made Simple. *Phys. Rev. Lett.* **1996**, 77, 3865–3868.
- (71) Hui, M.-H.; Ware, W. R. Exciplex Photophysics. V. The Kinetics of Fluorescence Quenching of Anthracene by N,N-Dimethylaniline in Cyclohexane. *J. Am. Chem. Soc.* **1976**, 98, 4718–4727.
- (72) Gould, I. R.; Young, R. H.; Mueller, L. J.; Albrecht, A. C.; Farid, S. Electronic Structures of Exciplexes and Excited Charge Transfer Complexes. *J. Am. Chem. Soc.* **1994**, 116, 8188–8199.
- (73) Birks, J. B.; Dyson, D. J. The Relations Between the Fluorescence and Absorption Properties of Organic Molecules. *Proc. R. Soc. London, Ser. A* **1963**, 275, 135–148.
- (74) Shida, T. *Electronic Absorption Spectra of Radical Ions*; Elsevier: Amsterdam, 1988; Vol. 34.
- (75) van Stokkum, I. H. M.; Larsen, D. S.; van Grondelle, R. Global and Target Analysis of Time-Resolved Spectra. *Biochim. Biophys. Acta, Bioenerg.* **2004**, 1657, 82–104.
- (76) Burshtein, A. I. Non-Markovian Theories of Transfer Reactions in Luminescence and Chemiluminescence and Photo- and Electrochemistry. *Adv. Chem. Phys.* **2004**, 129, 105–418.
- (77) Ivanov, A. I.; Burshtein, A. I. Luminescence Quenching by Reversible Ionization or Exciplex Formation/Dissociation. *J. Phys. Chem. A* **2008**, 112, 11547–11558.
- (78) Rosspeintner, A.; Vauthey, E. Bimolecular Photoinduced Electron Transfer Reactions in Liquids under the Gaze of Ultrafast Spectroscopy. *Phys. Chem. Chem. Phys.* **2014**, 16, 25741–25754.
- (79) Rosspeintner, A.; Lang, B.; Vauthey, E. Ultrafast Photochemistry in Liquids. *Annu. Rev. Phys. Chem.* **2013**, 64, 247–271.
- (80) Murata, S.; Matsuzaki, S. Y.; Tachiya, M. Transient Effect in Fluorescence Quenching by Electron Transfer. 2: Determination of

the Rate Parameters Involved in the Marcus Equation. *J. Phys. Chem.* **1995**, *99*, 5354–5358.

(81) Rosspeintner, A.; Angulo, G.; Vauthey, E. Bimolecular Photoinduced Electron Transfer Beyond the Diffusion Limit: The Rehm–Weller Experiment Revisited with Femtosecond Time Resolution. *J. Am. Chem. Soc.* **2014**, *136*, 2026–2032.

(82) Hamm, P. Coherent Effects in Femtosecond Infrared Spectroscopy. *Chem. Phys.* **1995**, *200*, 415–429.

(83) Murata, S.; Tachiya, M. Unified Interpretation of Exciplex Formation and Marcus Electron Transfer on the Basis of Two-Dimensional Free Energy Surfaces. *J. Phys. Chem. A* **2007**, *111*, 9240–9248.

(84) Kakitani, T.; Matsuda, N.; Yoshimori, A.; Mataga, N. Present and Future Perspectives of Theoretical Aspect of Photoinduced Charge Separation and Charge Recombination Reactions in Solution. *Prog. React. Kinet.* **1995**, *20*, 347–381.

(85) Vauthey, E.; Parker, A. W.; Phillips, D.; Nohova, B. Time Resolved Resonance Raman Study of the Rate of Separation of a Geminate Ion Pair into Free Ions in a Medium Polarity Solvent. *J. Am. Chem. Soc.* **1994**, *116*, 9182–9186.